Incorporating Residual Stresses in Life Prediction of Turbine Engine Disks

Reji John, James M. Larsen
Air Force Research Laboratory
Materials and Manufacturing Directorate
AFRL/MLLMN, 2230 Tenth Street, Suite No. 1
Wright-Patterson Air Force Base, Ohio 45433-7817, U.S.A.

Dennis J. Buchanan, Noel E. Ashbaugh
University of Dayton Research Institute
300 College Park, Dayton, Ohio 45469, U.S.A.

ABSTRACT

The U.S. Air Force has initiated a technology development initiative known as Engine Rotor Life Extension (ERLE), which has the goal of extending the useful lifetime of major, fracture-critical components in currently fielded gas turbine engines, without increasing the risk of component failure. Full achievement of this goal will require improvements in a broad range of technologies, including life prediction and fracture mechanics, nondestructive evaluation, engine usage and health monitoring, and component repair. This paper focuses on a key aspect of the life prediction process – the incorporation of residual stress effects. The benefits of compressive residual stresses in improving fatigue life, retardation of crack growth and resistance to foreign object damage have been demonstrated. Hence, these beneficial surface treatments are extensively employed in the turbine engine components. However, current damage-tolerance-based life management practices do not explicitly account for the residual stresses induced by surface enhancement procedures. Significant increase in predicted damage tolerance can be obtained if residual stresses are included in the life prediction methodology. This paper provides an assessment of the role of residual stresses in the durability of the component and identifies critical issues to be addressed during implementation in life prediction methods.

INTRODUCTION

The U.S. Air Force has initiated a technology development initiative known as Engine Rotor Life Extension (ERLE) [1], which has the goal of extending the useful lifetime of major, fracture-critical components in currently fielded gas turbine engines, without increasing the risk of component failure. A broad range of related technologies such as life prediction and fracture mechanics, nondestructive evaluation, engine usage and health monitoring, and component repair have been targeted for achievement of this goal. The total life of an engine component can be determined as the sum of crack initiation life and crack propagation life. Crack propagation life typically includes the short and long crack growth regimes. Current life management practice (Engine Structural Integrity Program, ENSIP) [2,3] by the U.S. Air Force uses a damage-tolerance-based method for managing the life of safety-critical components. This approach is based on systematic inspections of critical life-limiting locations in components. The inspection intervals are determined as 50% of the predicted crack growth life from an assumed initial crack growth size. Using nondestructive inspection (NDI) techniques, the components are inspected for location-specific crack sizes. The

Paper presented at the RTO AVT Symposium on "Ageing Mechanisms and Control: Part B – Monitoring and Management of Gas Turbine Fleets for Extended Life and Reduced Costs", held in Manchester, UK, 8-11 October 2001, and published in RTO-MP-079(I).

component design lifetime is based on a crack initiation criterion, but if a crack is detected prior to this mandatory component retirement lifetime, then the component is retired immediately.

The prediction of the crack length versus cycles behavior at critical locations in a component is based on the expected thermo-mechanical loading conditions and the assumed crack growth behavior of material. Prior to insertion in service, most critical locations, such as holes, stress concentration sites, etc., are subjected to surface enhancement procedures such as shot peening. Most of the legacy engines used shot-peening to retard crack growth at critical locations. Shot-peening introduces significant near-surface (within 150-200 μm) compressive stresses. The benefits of these compressive residual stresses in improving fatigue life, retardation of crack growth and resistance to foreign object damage have been extensively demonstrated. However, current damage-tolerance-based life management practices, i.e. predictions of crack initiation life and crack propagation life, do not explicitly account for the residual stresses induced by surface enhancement procedures. In current engines, shot-peening is used as a bonus factor of safety, resulting in potentially excessive conservatism in the component life prediction. Hence, incorporating residual stresses in crack growth life prediction is a key life extension technology. This paper provides an assessment of the role of residual stresses in the durability of the component and identifies critical issues to be addressed during implementation in life prediction methods.

MATERIAL

One of the materials used in components under consideration for life extension is Ti-6Al-2Sn-4Zr-6Mo (weight %) (Ti-6246). This material was forged and heat treated to produce a fine duplex microstructure of equiaxed primary α phase (hexagonal close packed) in a matrix of Widmanstatten α + β (body-centered cubic) phase as shown in Figure 1.

The analysis of crack growth in the presence of residual stresses requires characterization of baseline crack growth behavior of the material over a wide range of stress ratios, R. Hence, fatigue crack growth experiments were conducted using standard compact tension, C(T) geometry and single edge cracked geometry with clamped ends, CSE(T). The C(T) specimen was used for R = 0.1, 0.2, 0.3, 0.5, 0.6, 0.7, 0.8 and 0.9, and the CSE(T) specimen was used for R=-0.5 and −1.0. The crack growth data were acquired under decreasing stress-intensity-factor-range, ΔK, fatigue followed by constant-load amplitude fatigue. The resulting fatigue crack growth rate data were fit using Eqn. (1).

$$\log\left(\frac{da}{dN}\right) = C_1\left\{\arctan h\left(C_2\left[\log(\Delta K) + C_3\right]\right)\right\} + C_4 \qquad (1)$$

in which,

$$C_i = A_{0i} + A_{1i}\log(1-R) + A_{2i}\left[\log(1-R)\right]^2 . \qquad (2)$$

The baseline crack growth behavior of Ti-6246, as described by Eqn. (1), is shown in Figure 2 for the range $-1 \le R \le 0.8$. In obtaining the constants A_{0i}, A_{1i} and A_{2i}, the fracture toughness of Ti-6246 was set equal to 28 MPa$\sqrt{m}$, based on the data. Note that, in Figure 2, $\Delta K = K_{max} - K_{min}$ for all R. The threshold stress intensity factor range, ΔK_{th}, is ≈ 1.5 – 4 for all R. Hence, the near-threshold crack growth response of materials with such low values of ΔK_{th} can be expected to be influenced significantly by residual stresses, even if the magnitude of residual stress is low.

SHOT PEEN INDUCED RESIDUAL STRESSES

Shot peening induced residual stress (σ_{res}) distributions for Ti-6246 were unavailable in the open literature. Hence, we estimated the residual stress distribution as a function of depth based on available data on similar materials such as Ti-6Al-4V. The magnitude of the residual stress distribution was estimated using the ratio of the yield stresses of the materials (≈1170 MPa for Ti-6246 and ≈950 MPa for Ti-6Al-4V). The estimated σ_{res} for Ti-6246 is shown in Figure 3 for four shot peening intensities. Extensive data for various materials available in the literature show that the surface residual stress is typically lower than the sub-surface peak value. The magnitude of the surface residual stress depends on many factors such as shot-peening intensity, shot-peening coverage, surface finish prior to shot peening, material hardening behavior, etc. Hence, based on available data, the surface stress was conservatively assumed to be 50% of the sub-surface peak value.

Using the weight function method, the stress intensity factor due to residual stresses, K_{res} was determined for a semi-elliptical surface with surface crack length = 2c (tip-to-tip), crack depth = a, and aspect ratio, a/c=1. K_{res} at the surface crack tip (c), $K_{res,c}$, and at the deepest point in the depth direction (a), $K_{res,a}$, is shown in Figure 4 corresponding to the σ_{res} distributions shown in Figure 3. Since residual stresses are compressive, the computed K_{res} is mathematically negative. While the authors recognize that a negative K_{res} has no formal meaning, negative K_{res} is used to describe the relative magnitude of the compressive stress across the crack surfaces. K_{res} is always added to the applied K, and the total K = applied K + K_{res} should be positive for crack growth to occur. The magnitude of $K_{res,c}$ and $K_{res,a}$ are in the same range or higher than ΔK_{th} for a = 50 – 300 μm. Hence, in this regime of crack growth, significant influence of σ_{res} on the crack length versus cycles response can be expected. $K_{res,c}$ reaches a maximum at c ≈ 200 μm and remains constant up to c = 1000 μm. In contrast, $K_{res,a}$ reaches a maximum at c = a ≈ 100 μm and decreases to ≈0 at c = a ≈ 600-1000 μm. This difference between $K_{res,c}$ and $K_{res,a}$ implies that, in the presence of residual stresses, minimal crack extension might be observed on the surface while the crack is growing inside the specimen.

During service, the turbine engine components are subjected to complex thermal and mechanical loading conditions. Numerous studies using coupon-type specimens have shown that residual stresses relax during thermal exposure and fatigue loading [for example, 4-9]. Most of the data available are based on surface residual stress measurements. However, accurate prediction of crack growth requires the knowledge of residual stress distribution as a function of depth. Recent work by Cao et al. [6] and Prevey et al. [7,8] report residual stress distributions as a function of exposure time. Figure 5(a) shows the relaxation of residual stresses in Ti-6Al-4V at 325°C [7]. Rapid and significant relaxation (≈50%) is observed near the surface during the first ten minutes and the distribution remains relatively stable beyond 10 minutes. Similar results were also reported by Cao et al. [6] for a Ni-base superalloy (Astroloy) at 650°C. An important feature to be noted is that most of the relaxation of the residual stresses is confined to ≈ 100 μm below the surface.

Recently, Vukelich et al. [10] reported the results of residual stress measurements at various locations in Ni base superalloy engine disks, as shown in Figure 5(b). These disks had been subjected to complex thermal and mechanical loading conditions during service. These data are a compilation of measurements from numerous disks. Hence, the initial residual stresses (post shot-peen, pre-service) and the subsequent relaxation during service were not tracked at the same location and on the same component. Although there is significant scatter in the results, the data clearly show that, even after 8000 TACs (Total Accumulated Cycles), the minimum retained surface residual stress is ≈30-50% of the initial level.

The above results show that a wide variation in the magnitude of retained residual stresses can be expected during service. Hence, this paper is directed towards an assessment of the influence of residual stresses on the remaining crack propagation life and the effect of various degrees of retention of residual stresses. Incorporation of residual stresses in prediction of crack growth life requires accurate models to predict the relaxation of residual stresses during service. A few relaxation models [6,9] have been developed for a limited range of temperatures and mechanical loading. Additional extensive testing and modeling are required for accurate prediction of the true rate of decrease in the residual stresses under a wide range of thermal and mechanical loading conditions. Available data indicate that the most substantial residual stress relaxation occurs during the initial cycles. Hence, during this study, crack growth analysis was conducted for various levels of retained residual stresses as a percentage of the original stress distribution, as shown in Figure 6(a). This approach will result in conservative predictions for surface initiated cracks because as shown in Figure 5(a) most of the measured residual stress relaxation is restricted to the initial ≈100μm beneath the surface. The corresponding $K_{res,c}$ and $K_{res,a}$ are shown in Figure 6(b). Note that even an assumption of 50% retention of residual stresses results in K_{res} of ≈ -4 to –8 MPa$\sqrt{m}$ for crack sizes of ≈ 50 to 200 μm. These K_{res} values are of the same order of magnitude as ΔK_{th}, and hence, the retained residual stresses are sufficient for significant crack growth retardation. The influence of retained residual stresses on fatigue limits and crack propagation life is discussed next. In the following sections, the long-crack growth behavior shown in Figure 2 was used for analysis of small cracks. For cracks greater than ≈ 25μm, this assumption was previously shown to be valid based on experiments on naturally initiated small surface cracks in Ti-6246 [11,12].

RESIDUAL STRESS EFFECTS ON THRESHOLD STRESS AND FLAW SIZE

The influence of residual stresses on the threshold crack size corresponding to no-growth conditions was studied by utilizing a Kitagawa-Takahashi [13] type plot of maximum stress versus flaw size. Such a plot corresponding to R=0.1 and R=0.8 is shown in Figure 7(a) and 7(b), respectively. These stress ratios bound the typical stress ratios experienced by some of the life extension candidate components. The maximum stress is bounded by the fatigue limit (typically 10^7-cycle fatigue limit) [14] and the stress-crack length relationship defined by the threshold stress intensity factor range, ΔK_{th}. A similar approach was used by Larsen et al. [14,15] to generate fatigue life maps and to assess the influence of residual stresses on threshold crack sizes. At R=0.1 and 0.8, if the assumed initial flaw depth exceeds 10 and 30 μm, respectively, the threshold stress (fatigue limit) decreases with increasing flaw size per LEFM equations. Figure 7 also shows the predictions for threshold stress in the presence of residual stresses corresponding to intensities of ~ 4A and ~16A. The predictions for the two shot peening intensities are nearly similar and clearly shows the substantial increase in the fatigue limit for a given flaw size. For a flaw size ≈ 100 μm, at R=0.1 and 0.8, the threshold stress ≈ 200 and 500 MPa, respectively, in the absence of residual stresses. These threshold-stresses increase to the respective upper bound fatigue limit in the presence of the residual stress. For a stress level of ≈ 200 MPa, the threshold flaw size increases from ≈ 100 μm to ≈ 400 μm. Thus, the safe region for the no-growth condition is increased substantially by the residual stresses. Although, the threshold flaw size at R=0.8 is higher than that at R=0.1 for a given stress, the subsequent benefit of the residual stresses is significantly lower than that at R=0.1. Figure 7 also shows that the benefits of the residual stresses vanish for flaw size greater than 600-700 μm. This result is consistent with the predicted near-zero $K_{res,a}$ for flaw sizes greater than 600-700 μm, as shown in Figure 4(b).

As discussed earlier, shot-peening induced residual stresses relax during service. Hence, the threshold stress for two flaw sizes were determined for various levels (0 to 100%) of the residual stress corresponding to ~8A intensity, as shown in Figure 8(a). The corresponding residual stress

distribution was shown in Figure 6. Under LCF conditions (R=0.1), for a flaw size of 120 μm, the threshold stress is ≈ 150% higher than the baseline stress even at residual stress retention of only 50%. For a flaw size of 25 μm, the threshold stress at R=0.1 is ≈ 40% higher than the baseline. Therefore, the larger flaw size exhibits a higher increase of threshold stress. At R=0.8, even though the relative increase is lower than that for R=0.1, the retained threshold stress is still higher than the baseline value. The sensitivity of the threshold flaw size corresponding to stress = 500 MPa to the level of residual stress is shown in Figure 8(b). Corresponding to the baseline value, at 100% of residual stress, the threshold flaw is ≈ 10X and 2X higher at R=0.1 and 0.8, respectively. Even with only 50% retention of the residual stress, the threshold flaw size is still greater than the current NDE limit (≈ 125 μm) for some components. The results in Figure 8 clearly show that 50% retention of residual stresses is sufficient to generate substantial increases in threshold stress and flaw size. In this calculation, the entire residual stress distribution was assumed to decrease by the same percentage. As discussed earlier, Figure 5(a), the bulk of the relaxation occurs near the surface. Hence, the actual retained residual stress benefits can be expected to be higher than that predicted in Figure 8. The benefits of residual stresses on the crack propagation life are discussed next.

RESIDUAL STRESS EFFECTS ON CRACK GROWTH BEHAVIOR

The ENSIP design philosophy assumes that a 794 μm (=1/32 in.) flaw could initiate during service in 1 out of 1000 components. In addition, ENSIP requires that the remaining crack propagation life from an inspectable crack size be equal to the component design life. This life management practice relies on accurate prediction of the crack growth behavior at critical locations and the ability to define safe inspection intervals based on this prediction. Current crack growth predictions exclude the influence of beneficial compressive residual stresses. Extensive data and analyses are available in the literature highlighting the significant increase in crack propagation life due to residual stresses. As discussed earlier, residual stresses relax, and significant scatter exists in the retained residual stresses. Hence, prior to implementation of the residual stresses in component lifing, the sensitivity of crack propagation life to various levels of residual stresses should be assessed. Extensive crack growth analyses were conducted for a semi-elliptical surface crack in an infinite geometry. The crack growth analysis code AFGROW [16] was used during this study. Equations (1) and (2) were used to generate a tabular database to represent the crack growth behavior of the material in AFGROW.

Figures 9(a) to 9(c) show the predicted maximum stresses versus crack propagation life, N_p, for two initial flaw sizes (25 and 120 μm) and residual stress levels corresponding to 20 and 50% of 8A. In actual components, the amount of retained residual stresses can be expected to be dependent on the applied stresses. The relaxation occurring at locations with high stresses (close to yield) will be the maximum. In this analysis, we assumed that the extent of relaxation is independent of stress level. The results from Figures 9(a) to 9(c) are summarized in Figure 9(d), which shows the ratio of N_p to N_p corresponding to σ_{res}=0 as a function of maximum applied stress. At R=0.1, this ratio ranges from 2 to 50 depending on the stress level and initial flaw size. The smaller the initial crack size, the higher is the relative gain in N_p. For initial flaw size of 25 μm, under LCF conditions (R = 0.1), 20% retention of the residual stress was sufficient to retain 5X to 50X increase in N_p compared to the baseline. Relative life gain higher than 2X at the high stress level for flaw size of 120 μm required 50% retention of the residual stresses. Under HCF conditions (R=0.8), the relative gain at high stress levels is less than 2X for residual stress retention of 50%. The lower gain in N_p at R=0.8 is consistent with similar observations of crack growth in residual stress fields in the literature [17]. The data shown in Figure 5(b) exhibited residual stress retention of ≈ 30-50%, based on surface measurement. The calculations were conducted assuming that the entire stress distribution decreased by the same percentage, in contrast to the data. Hence, the predictions shown in Figure 9 may be considered conservative, considering observations similar to those in Figure 5(a).

The crack growth response (surface crack length and crack depth versus cycles) at 600 MPa / R=0.1 corresponding to σ_{res} = 0 and 50% 8A is shown in Figure 10(a) and 10(b), respectively. The initial flaw size was c_i = 120 μm and the initial aspect ratio was a_i/c_i = 1.0. In the absence of residual stresses, this surface crack grows such that the aspect ratio nearly remains the same. In addition, at half-life, c has increased from 120 μm to ≈ 210 μm. Hence, the detectability of this crack has increased significantly at the end of the half-life period. In contrast, in the presence of residual stresses, the surface crack shows negligible crack growth almost up to 90% of total life. This response is similar to the response under HCF loading conditions. In the depth direction, there is marked increase in the rate of crack growth at ≈ 67% of life. This distinct difference in the crack growth response in the presence of σ_{res} compared to that in the absence of σ_{res} identifies a critical need for a more accurate and reliable NDI technique, which is sensitive to the crack extension in the surface and depth directions.

The influence of retained residual stresses on crack growth in the presence of combined LCF-type and HCF-type cycles is shown in Figure 11. Crack propagation life for an initial crack size of 120 μm subjected to maximum stress = 625 MPa was predicted for various ratios of number of cycles at R=0.8 to number of cycles at R=0.1. The retained residual stress distribution was assumed to be 30% of 8A. Also shown in Figure 11 is the baseline prediction (σ_{res}=0) and the trend-line corresponding to two times the baseline predictions. The crack propagation life in the presence of σ_{res} was always greater than twice that of the baseline, even for the case with high number of HCF-type cycles. Note that at stress levels close to the yield stress, the retained residual stresses may be significantly lower than 50%. In this case, the higher number of HCF-type cycles result in significantly reduced residual stress benefits on crack propagation life.

REMARKS

The properties used during this study are based on the original material prior to insertion in service. During service, the *in situ* properties of the material could change. Hence, analysis conducted to predict the remaining life should account for the current material behavior and the anticipated changes in these properties. Fractographic examinations of post-service components are in progress to assess the changes in the microstructure during service. Following these examinations, crack growth behavior will be characterized on specimens extracted from these components.

Successful incorporation of residual stresses in life management will require a good understanding of the surface and sub-surface residual stress changes. As mentioned earlier, only limited data [e.g. 6-8] are available documenting sub-surface residual stress changes. Vuckelich et al. [10] reported the first work documenting surface residual stress changes from detailed measurements on actual components. This work provided an idea of the range of relaxation of residual stresses that can be expected during service. However, accurate prediction of crack growth life requires sub-surface residual stress distributions also. Hence, additional data from destructive sub-surface measurements need to be collected.

The results of this study show that even retention of only 30% of the original residual stress distribution can yield greater than 2X increase in crack growth life, compared to the current baseline predictions, which exclude residual stresses. Data from laboratory coupon specimens and recent field inspection studies have shown that residual stresses can be expected to relax in most components. Thus, combining data from the field with detailed laboratory experiments and analysis, a reduced level of residual stress can be established and implemented in life management practice. Monitoring residual stresses at critical locations during service can help reduce the potential increase in risk associated with disk life extension. Life management based on such threshold residual stress level

will require NDI-based accurate monitoring of residual stress at critical locations. Recent depth measurements have shown that the most substantial residual stress relaxation occurs close to the surface. Sub-surface residual stress relaxation is not as severe as that observed on the surface. Hence, the NDI techniques should be capable of sub-surface residual stress measurement, preferably up to 150 μm deep. Note that such residual stress inspections are in addition to current crack inspections being conducted under the ENSIP program. Therefore, successful implementation of a life prediction methodology using residual stresses requires two critical NDI technology developments. These are: (1) accurate and reliable NDI techniques sensitive to crack extension in the surface and depth directions, and (2) NDI techniques to monitor surface and subsurface changes in residual stresses in components.

Surface enhancement procedures, such as shot peening, retard or prevent surface crack growth. Hence, if the lives of some of the components are extended, at certain locations, the chances of sub-surface crack initiation and growth are increased. Additional testing and analysis are required to characterize and model this behavior. New NDE techniques for detecting sub-surface crack initiation and growth may also be required to mitigate the increased risk of failure at these locations.

The results from this study show that substantial gains in crack propagation life can be realized if residual stresses are included in the life prediction methodology. This would require: (1) adequate quality control during the surface enhancement procedure, (2) understanding of changes in the residual stress distribution (surface and depth) during service, (3) accurate life prediction with residual stresses, and (4) monitoring of surface and depth residual stress periodically during service, similar to current crack inspection procedures. The utilization of residual stresses in the engine life management practice is also a key technology necessary for developing longer life and durable engines. Introduction of residual stresses via newer procedures such as low plasticity burnishing (LPB) [18] and laser shock peening (LSP) [19] are being explored. The retention of residual stresses generated by LPB and LSP have been reported to be significantly better than that generated by shot peening because of the reduced cold work [7,8]. Hence, re-introduction of residual stresses in legacy engine components using LPB and LSP should also be explored.

SUMMARY

Life extension of fracture critical parts is under consideration by the US Air Force. This technology development initiative is expected to significantly reduce the sustainment burden and to enable future long-life durable engines. Data from legacy engines indicate that shot-peen induced residual stresses at critical locations are retained only partially during service. This paper assessed the influence of various levels of retained residual stresses on the threshold stresses, threshold crack sizes and crack propagation in Ti-6Al-2Sn-4Zr-6Mo. The results show that even retention of only 30% of the original residual stress distribution can yield greater than 2X increase in crack growth life compared to the baseline predictions excluding residual stresses. Thus, combining data from the field with detailed experiments and analysis, a threshold level of location-specific residual stress can be established and implemented in the life management practice. The inclusion of residual stresses in life prediction of the component will require NDI-based accurate monitoring of residual stress at life-limiting critical locations, in addition to crack inspections being conducted under the ENSIP program. The NDI techniques should enable monitoring of surface and sub-surface residual stresses. Improved NDI techniques, sensitive to surface and depth crack growth, are also required.

ACKNOWLEDGMENTS

This research was performed in the Air Force Research Laboratory, Materials and Manufacturing Directorate (AFRL/MLLMN), Wright-Patterson Air Force Base, OH, USA.

REFERENCES

1. Larsen, J.M. et al., "The Engine Rotor Life Extension (ERLE) Initiative and It's Opportunities to Increase Life and Reduce Maintenance Costs," presented at AeroMat 2001, Long Beach, CA, 12 June 2001.
2. Harris, J.A., "Engine Component Retirement for Cause, Vol. I - Executive Summary," AFWAL-TR-87-4069, Vol. I., Air Force Wright Aeronautical Laboratories," Wright-Patterson AFB, OH, 1987.
3. Engine Structural Integrity Program (ENSIP), MIL-STD-1783 (USAF), 30 November 2001.
4. Holzapel, H., Schulze, V., Vohringer, O., and Macherauch, E., "Residual Stress Relaxation in an AISI 4140 Stell due to Quasi-static and Cyclic Loading at Higher Temperatures," Materials Science & Engineering, Vol. A248, pp. 9-18, 1998.
5. Berger, M.-C and Gregory, J.K., "Residual Stress Relaxation in Shot Peened Timetal®21S," Materials Science and Engineering, Vol. A263, pp. 200-204, 1999.
6. Cao, W., Khadhraoui, M., Brenier, B., Guedou, J.Y., and Castex, L., "Thermomechanical Relaxation of Residual Stress in Shot Peened Nickel Base Superalloy," Material Science and Technology, Vol. 10, pp. 947-954, November 1994.
7. Prevey, P., Hornbach, D., and Mason, P., "Thermal Residual Stress Relaxation and Distortion in Surface Enhanced Gas Turbine Engine Components," Proceedings of the 17th Heat Treating Society Conference and Exposition and the 1st International Induction Heat Treating Symposium, D.L. Milam et al., Eds., ASM, Materials Park, OH, pp. 3-12, 1998.
8. Prevey, P., "The Effect of Cold Work on the Thermal Stability of Residual Compression in Surface Enhanced IN718," Proceedings, 20th ASM Materials Solutions Conference & Exposition, St. Louis, Missouri, Oct. 10-12, 2000.
9. Ahmad, J., Chandu, S., and Prevey, P., "An Analysis of Redistribution of Surface Treatment Induced Residual Stresses", To be submitted for publication, 2001.
10. Vukelich, S., Russ, S.M., Berkley, S., and Bradley, E.F., "Residual Stress Measurement and it's Application to Achieve Predicted Full Life Potential of Low Cycle Fatigue (LCF) Limited Engine Disks," The 9th International Symposium on Transport Phenomena and Dynamics of Rotating Machinery, Honolulu, Hawaii, February 10-14, 2002.
11. Larsen, J.M. and Jira, J.R., Experimental Mechanics, pp. 82-87, 1991.
12. Jira, J.R., Nicholas, T., and Larsen, J.M., Fatigue 87, Vol. IV, E. Starke and R.O. Ritchie, Eds., Engineering Materials Advisory Services, Ltd., West Midlands, U.K., pp. 1851-1860, 1987.
13. Kitagawa, H. and Takahashi, S., Proceedings of the Second International Conference on Mechanical Behavior of Materials, Boston, MA, pp. 627-631, 1976.
14. Larsen, J.M., Russ, S.M., John, R., and Maxwell, D.C., "The Role of Threshold Fatigue Crack Growth in Life Prediction of Two Titanium Alloys Under High Cycle Fatigue Spectra," To be submitted for publication, 2001.
15. Larsen, J.M., John, R., Russ, S.M., Maxwell, D.C., Worth, B.D., Rosenberger, A.H., Li, K. and Porter, W.J., "The Role of Near-Threshold Small-Crack Behavior in Life Prediction of Titanium Alloys For Use in Advanced Turbine Engines," Small Fatigue Cracks: Mechanics and Mechanisms, K.S. Ravichandran, R.O. Ritchie, and Murakami, Y., Eds., Elsevier Science, Oxford, UK, 1999.
16. AFGROW, Harter, J., US Air Force Research Laboratory, AFRL/VASM, Wright-Patterson Air Force Base, OH, USA. Available at http://fibec.flight.wpafb.af.mil/fibec/afgrow.html.
17. Ruschau, J.J., John, R., Thompson, S.R., and Nicholas, T., "Fatigue Crack Growth Characteristics of Laser Shock Peened Ti-6Al-4V" Journal of Engineering Materials and Technology, Vol. 121, No.3, pp. 321-329, 1999.
18. Prevey, P.S. and Cammett, J., "Low Cost Corrosion Mitigation and Improved Fatigue Performance of Low Plasticity Burnished 7075-T6," Proceedings, 4th International Aircraft Corrosion Workshop, Solomons, MD, Aug 22-25, 2000.
19. Clauer, A.H., "Laser Shock Peening for Fatigue Resistance," Surface Performance of Titanium, J.K. Gregory et al., Eds., TMS, Warrendale, PA, pp. 217-230, 1996.

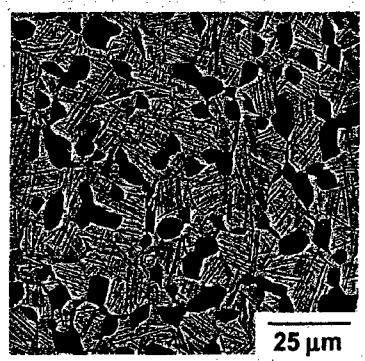

Figure 1. Fine, equiaxed $\alpha + \beta$ microstructure of Ti-6Al-2Sn-4Zr-6Mo after heat treatment.

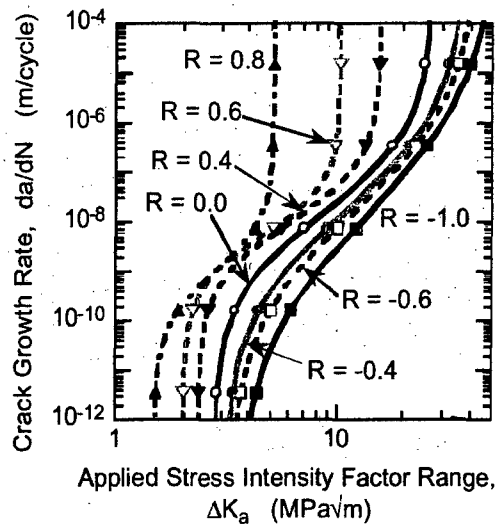

Figure 2. Baseline long crack growth behavior of Ti-6Al-2Sn-4Zr-6Mo. These curves are from Equation (1).

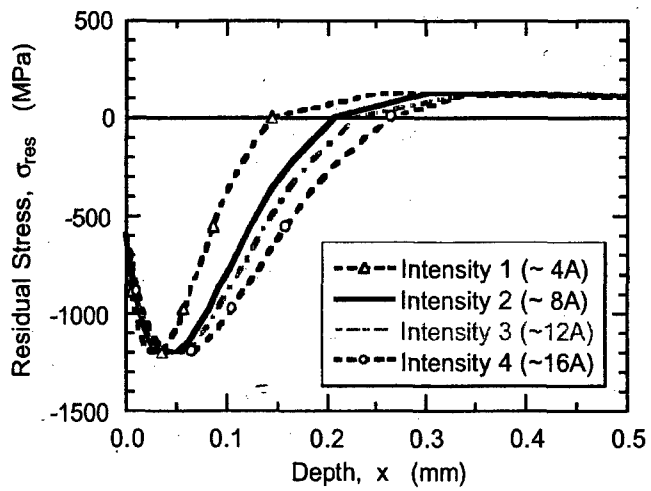

Figure 3. Estimated residual stress, σ_{res}, distributions in Ti-6Al-2Sn-4Zr-6Mo due to shot-peening.

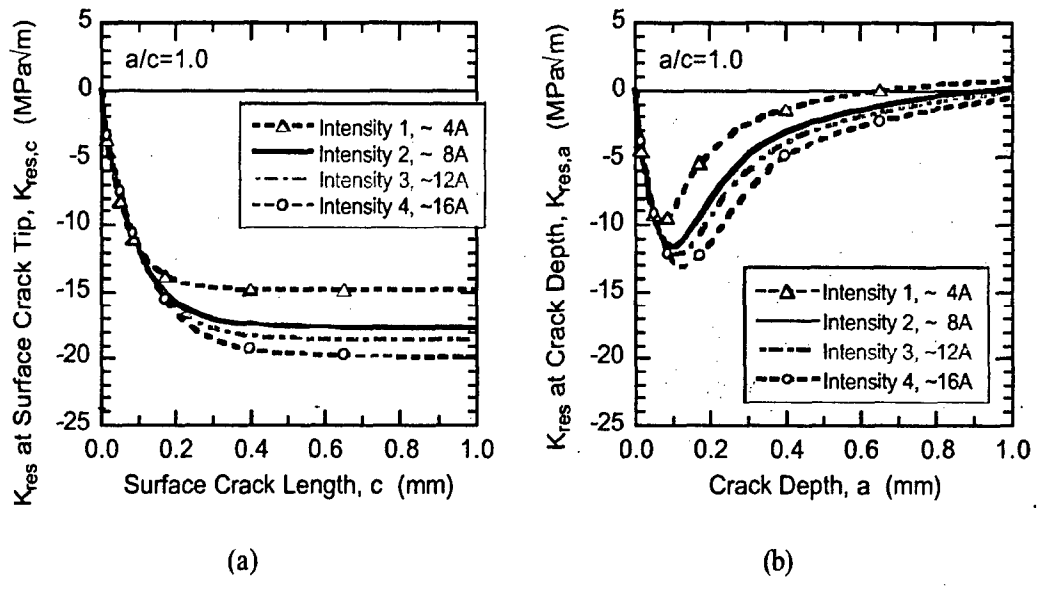

Figure 4. Residual stress intensity factor, K_{res}, for a semi-elliptical surface crack with aspect ratio (a/c) = 1, due to the residual stress distributions shown in Figure 3. (a) K_{res} at surface crack tip,c, and (b) K_{res} at crack depth, a.

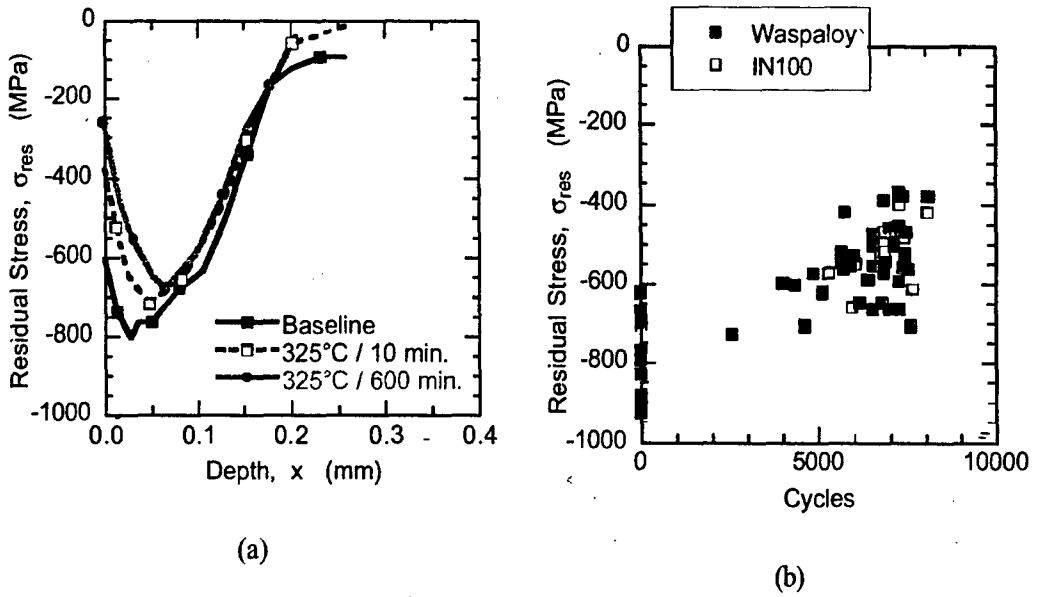

Figure 5. (a) Residual stress relaxation in Ti-6Al-4V at 325 °C [Prevey et al., 1998], and (b) Surface residual stress relaxation at notches in Ni-base superalloy engine disks [Vukelich et al., 2002].

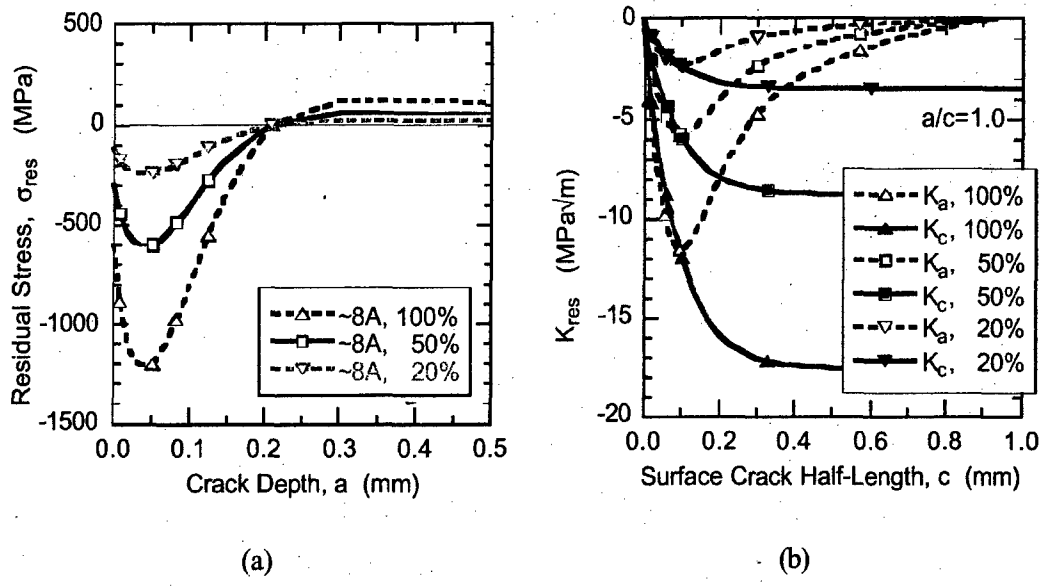

Figure 6. (a) Assumed residual stress distributions to simulate relaxation during service. (b) Corresponding $K_{res,c}$ and $K_{res,a}$ for aspect ratio, a/c=1.

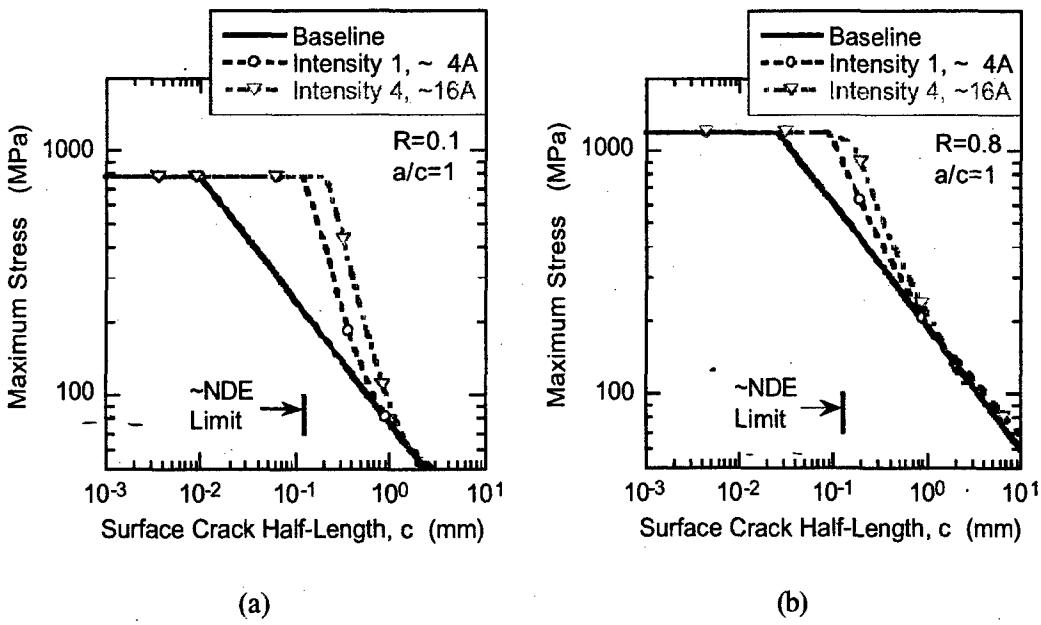

Figure 7. Predicted influence of shot-peen residual stresses on fatigue limit of Ti-6Al-2Sn-4Zr-6Mo at (a) R=0.1 and (b) R=0.8. Aspect ratio, a/c=1.

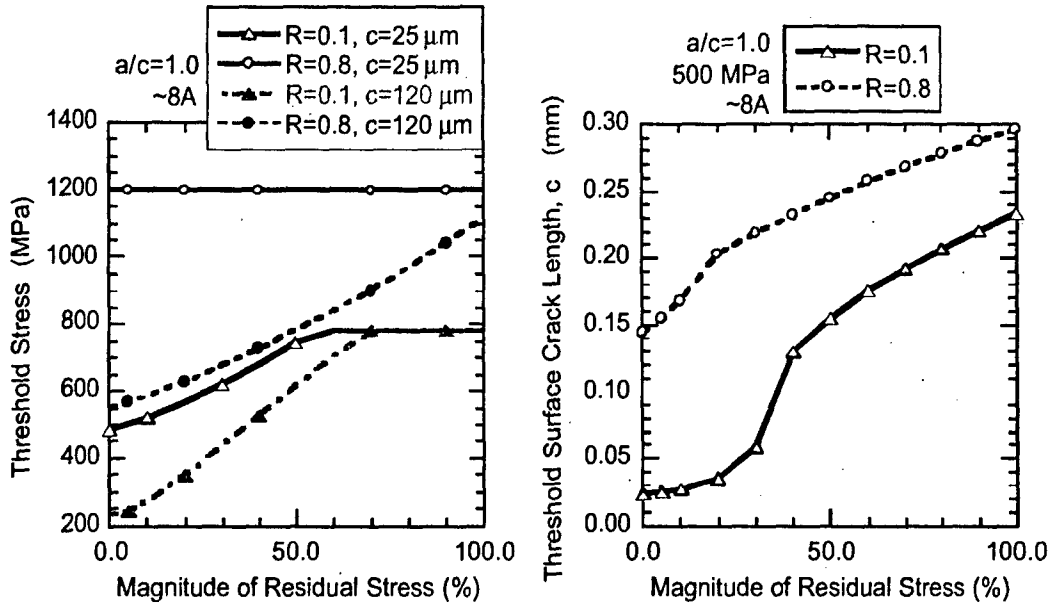

Figure 8. Influence of varying levels of residual stresses (0-100% of Intensity 2, ~8A) on (a) Threshold stress corresponding to c=25 and 120 μm, and (b) Threshold surface crack length corresponding to maximum applied stress = 500 MPa for a/c=1.0.

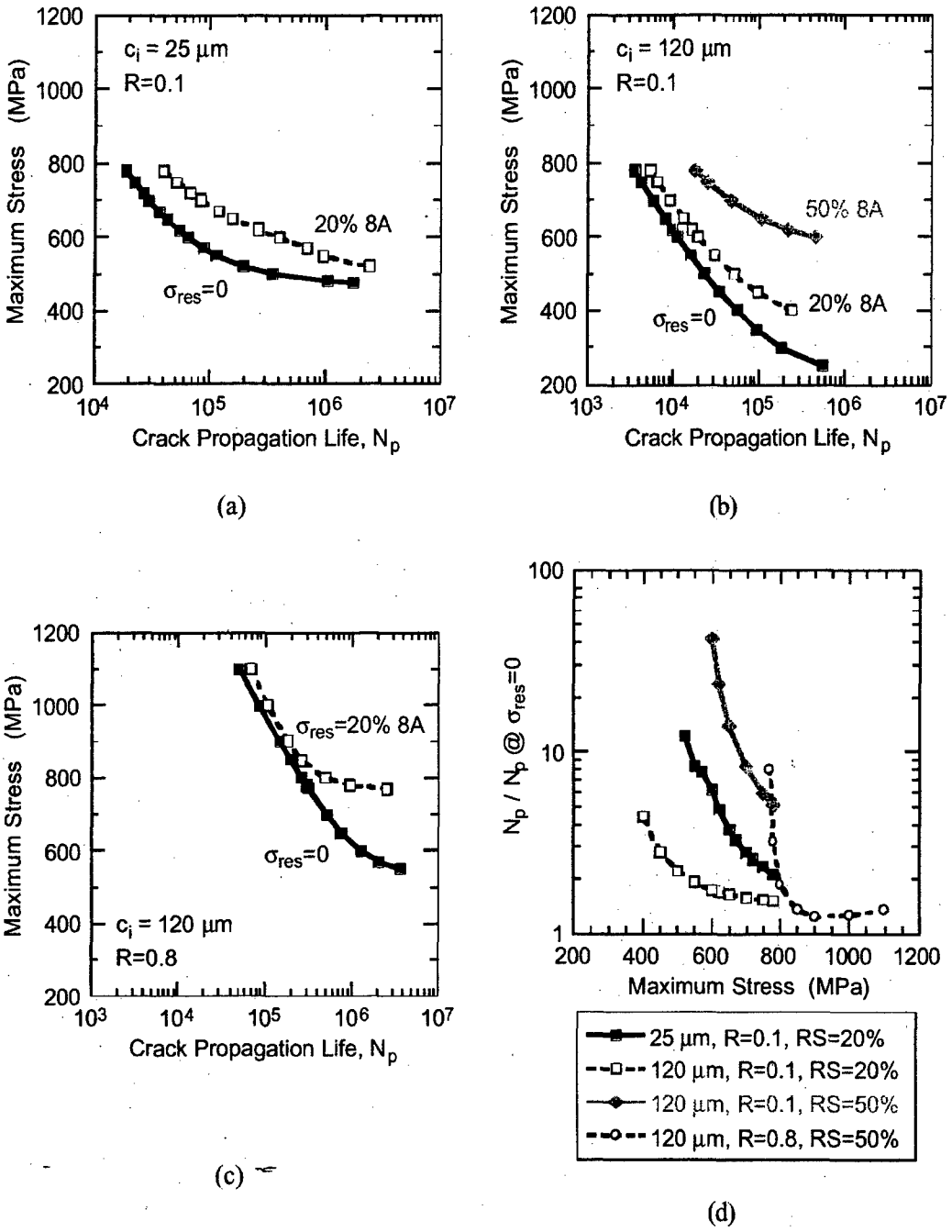

Figure 9. Predicted influence of retained residual stresses on crack propagation life (N_p). (a) Maximum stress versus propagation life (S-N_p) behavior at R=0.1 for $c_{initial}$=25 µm and a/c=1. (b) S-N_p behavior at R=0.1 for $c_{initial}$=120 µm and a/c=1. (c) S-N_p behavior at R=0.8 for $c_{initial}$=120 µm and a/c=1. (d) Ratio of N_p to baseline (σ_{res}=0) Np as a function of maximum stress.

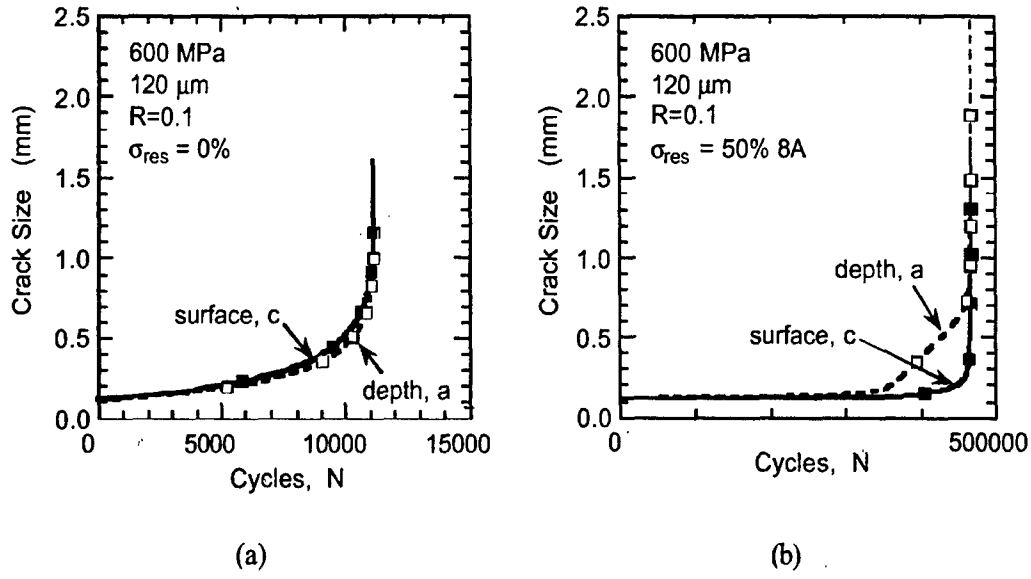

Figure 10. Crack growth behavior in the presence of residual stresses at R=0.1. (a) σ_{res} = 0, and (b) σ_{res} = 50% of 8A. Assumed initial crack size = 120 μm and initial a/c = 1.0.

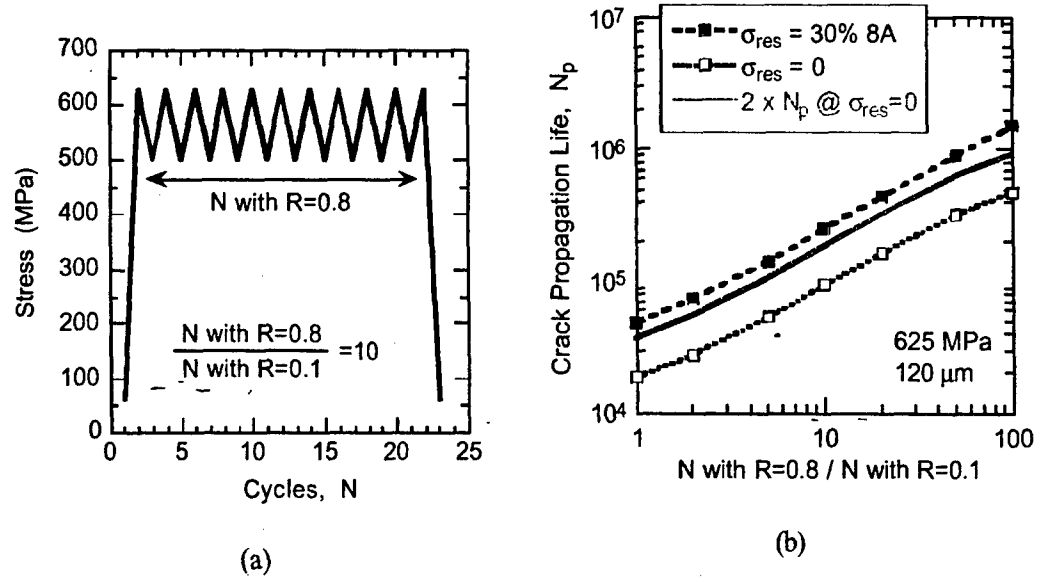

Figure 11. (a) Assumed simple mission loading sequence containing 1 R=0.1 cycle and multiple R=0.8 cycles. (b) Predicted crack propagation life, N_p. Assumed maximum stress = 625 MPa and initial crack size = 120μm.